Phys. Status Solidi B **253,** No. 12, 2499–2504 (2016) / **DOI** 10.1002/pssb.201600281

physica status solidi b
www.pss-b.com
basic solid state physics

THz time-domain spectroscopy and IR spectroscopy on MoS_2

David Arcos[1], Daniel Gabriel[1], Dumitru Dumcenco[2], Andras Kis[2], and Núria Ferrer-Anglada[*,1]

[1] Applied Physics Department, Universitat Politècnica de Catalunya (UPC), Campus Nord B4, J. Girona 3-5, 08034 Barcelona, Spain
[2] Electrical Engineering Institute, École Polytechnique Féderale de Lausanne (EPFL), Lausanne, Switzerland

Received 3 June 2016, revised 14 October 2016, accepted 18 October 2016
Published online 8 November 2016

Keywords conductivity, graphene, infrared spectroscopy, MoS_2, terahertz-time domain spectroscopy

[*] Corresponding author: e-mail nuria.ferrer@upc.edu, Phone: +34 934 016 880, Fax: +34 934 016 090

In the increasing research field of 2D materials such as graphene, molybdenum disulfide MoS_2 has attracted great interest due to the existence of a direct bandgap in monolayer MoS_2, which gives the possibility of achieving MoS_2 field-effect transistors or optoelectronic devices. We analyzed by THz time-domain spectroscopy (THz-TDS) up to 2 THz and infrared (IR) spectroscopy, CVD-obtained MoS_2 using either S or H_2S gas as a sulfur precursor, grown on a sapphire substrate. From THz-TDS we obtained the transmittance, conductivity, and attenuation. From IR spectroscopy on the same samples, we deduced the transmittance in the IR frequency range. We observed the coherence of both spectroscopic methods. The advantage of the THz-TDS method is that we can get significant parameters related to the sample quality without the need for depositing any electrical contact or sample preparation. Our results show that at high frequencies MoS_2 is even better than graphene as a material for optoelectronic devices.

1 Introduction Recent advances in fabrication of ultrathin layered materials down to atomic thickness have contributed toward the exploration of new low-dimensional physics.

Transition-metal dichalcogenides have attracted considerable attention due to their potential applications as new materials in the fields of catalysis, nanotribology, microelectronics, lithium batteries, medical and optoelectronics [1, 2] with applications as thin-film transistors, light-emitting diodes [3], or photodetectors [4]. In particular, molybdenum disulfide (MoS_2) is a two-dimensional material that recently has attracted increasing attention. In the bulk MoS_2 crystal, S–Mo–S layers are Van der Waals bonded [5], each of these layers (MoS_2 monolayer) can be considered as two hexagonal planes of S atoms and an intermediate hexagonal plane of Mo atoms bonded by covalent interactions with the S atoms in a trigonal prismatic structure (Fig. 1).

It is well known that bulk MoS_2 has an indirect bandgap of 1.29 eV, whereas the monolayer MoS_2 shows a direct bandgap of 1.80 eV.

Terahertz (THz) spectroscopy and imaging provides a powerful tool for the characterization of different kinds of materials, including semiconductors. In the last few years, there has been an increasing interest in THz imaging and spectroscopy for optoelectronic applications, and more and more THz characterization are being reported [7, 8].

Infrared spectroscopy (IR) analysis is important for its role in optoelectronic implementations. Both graphene and MoS_2 characterization in the THz and IR bands are a key requirement for its applications and development in optoelectronic devices.

2 Sample preparation and characterization We analyzed a total of four samples of pristine graphene transferred on a polyethylene terephthalate (PET) substrate and four samples of MoS_2 grown on sapphire substrates.

Graphene was obtained by chemical vapor deposition (CVD) transferred on a PET substrate and MoS_2 are obtained by CVD-S and CVD-H_2S, Table 1, described briefly in the next section. Samples S_1 were obtained at Sejong University as described in Ref. [9], and S_2 and S_3 are from the École Polytechnique Féderale de Lausanne (EPFL) as described in Ref. [10].

Structural quality, homogeneity, and domain size are described in Ref. [10] for MoS_2, and in Ref. [11] for graphene. The domain size is from 5 to 10 μm for MoS_2, and from 1 to 5 μm for graphene. Structural quality is tested by

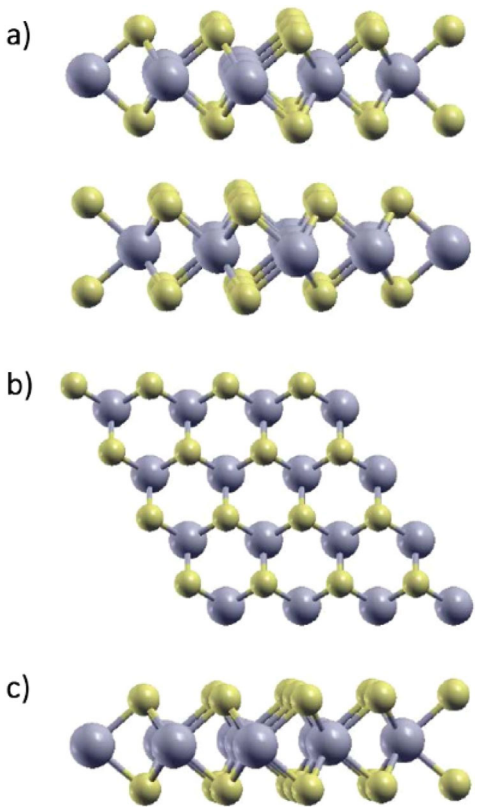

Figure 1 (a) Side view of bulk MoS_2. (b) Top view of bulk and monolayer MoS_2, Mo atoms are presented by spheres bigger than S. So for bulk MoS_2, the Mo atoms of the second layer must be seen. (c) Side view of monolayer MoS_2. The Mo atoms are depicted by gray and S atoms by yellow [6].

Raman spectroscopy, that shows good quality with low numbers of defects.

2.1 CVD-S MoS_2 and CVD-H_2S MoS_2 CVD is the most promising method to synthesize monolayer materials. In particular, MoS_2 can be obtained from triangular islands up to a large-scale film, depending on the growth conditions.

For sample CVD-S we used the common CVD method, which involves a solid sulfur source plus an inert gas (Ar) as a carrier gas flow. For CVD-H_2S we used a gas-phase precursor, a mixture H2S:H2 at different conditions of temperature and mixture ratio. Selecting both conditions allowed us to regulate the growth direction: when the injected gas temperature is 600 °C or lower and the ratio $H_2S{:}H_2 = 3{:}1$, the growth is horizontal and a centimeter-scale MoS2 monolayer is obtained, showing a morphology based on triangular-shaped domains that merge in a continuous film [10].

2.2 Raman characterization Raman spectroscopy is performed with an excitation laser of 532 nm, with a pinhole size of 150 μm, 100× objective, and a power of 0.5 mW that ensures the nondegradation of the sample. A quick and accurate sample identification (Fig. 2) is given by the Raman spectra.

Table 1 Summary of samples S_i, graphene or MoS_2 and their substrate, analyzed in the current study. Sample identification are used for later reference.

substrate	material	sample	growth	number of samples
PET	graphene	S_1	CVD	4
sapphire	MoS_2	S_2	CVD-S	2
sapphire	MoS_2	S_3	CVD-H_2S	2

Like graphene, single-layer and few-layer MoS_2 have distinctive signatures in its Raman spectrum. The Raman spectrum of bulk MoS_2 has two prominent peaks: an inplane mode (E^1_{2g} or E′ on Fig. 2) located around 383 cm^{-1} and an out-of-plane mode (A_{1g} or A'_1 on Fig. 2) that is located at 408 cm^{-1}. The E^1_{2g} line corresponds to the sulfur atoms vibrating in one direction and the molybdenum atom in the other, while the A_{1g} line corresponds to just the sulfur atoms vibrating out-of-plane. As MoS_2 becomes single layer, the inplane and out-of-plane modes, E^1_{2g} and A_{1g}, evolve with thickness. The inplane mode upshifts to 385 cm^{-1} and the out-of-plane downshifts to 403 cm^{-1} [12].

Both CVD-S and CVD-H_2S MoS_2 present similar Raman spectra but with some important differences. Both materials present an E^1_{2g} line located at 385.7 cm^{-1}, while the out-of-plane vibration, A_{1g}, is located at different frequencies, at 404.8 cm^{-1} (for sample CVD-S) and 405.3 cm^{-1} (for CVD-H_2S). The difference between A_{1g} and E^1_{2g} modes for both samples are ∼20 cm^{-1}, therefore, we can assume that both MoS_2 are monolayers [12]. The softening and broadening of the out-of-plane A_{1g} mode could be explained by different doping levels of MoS_2, increasing the doping level causes broadening of the A_{1g}

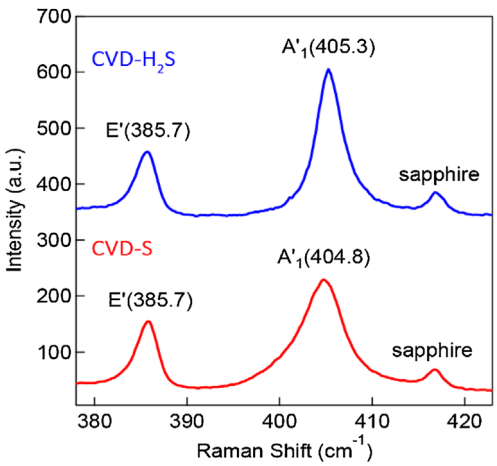

Figure 2 From top to bottom, Raman spectra of CVD-H_2S MoS_2, S_3, and CVD-S MoS_2, S_2, on sapphire substrate.

mode and decreases the intensity ratio between A_{1g} and E^1_{2g} modes, indicating in our case a higher doping level for sample CVD-S [13].

The different A_{1g} mode position in Raman spectra between the presented CVD-S and previous results corresponds to slightly different growth conditions of MoS_2 [14].

Raman spectra were taken using different sample zones, from 5 to 10 different points. In most of them the spectra are similar.

3 Experimental

3.1 THz time-domain spectroscopy Terahertz time-domain spectroscopy (THz-TDS) is a contactless, nondestructive spectroscopic technique based on a coherent detection scheme. Complex material properties can be measured at THz frequencies, up to 2 THz, by using a phase-sensitive technique. The THz measurements are collected using a THz-TDS spectrometer in transmission setup, based on the commercial TERA K8, from Menlo Systems (Fig. 3).

Broadband THz radiation is generated by using a 780-nm wavelength fs laser and is later detected with a photoconductive antenna. The output of the laser is split into a pump (generating) and a probe (detecting) beam using a polarizing beam splitter, where each of these beams travel through two different optical paths to the emitter and the detector antenna, respectively.

The probe (detecting) path implements a variable length using a delay line, to control the pulses delay arriving to the receiver antenna.

The pump (generating) beam is collimated to the emitter antenna with the purpose of producing a THz electric field that is transmitted through the sample and is modified by its frequency response. The beam spot size at the sample surface is about 550 μm, after the Menlo Systems specifications, but it could be slightly larger, close to 1 mm, when working. The modified electric field is focused on a THz detector photoconductive antenna, which is gated by the probe (detection) laser beam. As a result, a time-domain electric field pulse is obtained. The recorded time-domain trace is transformed into the frequency domain by using the Fourier transform (FFT) for spectroscopic analysis. From the frequency spectra, the refractive index, the conductance and attenuation of the sample can be deduced.

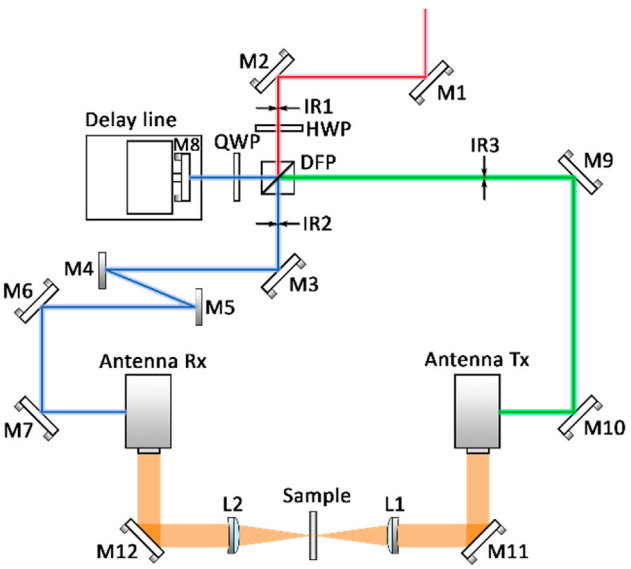

Figure 3 THz-TDS transmission setup configuration.

3.2 THz-TDS experimental results We analyze, using the THz time-domain spectroscopy, the conductivity of different MoS_2 samples grown on sapphire and, just for comparison, CVD-obtained graphene [11] transferred on a PET substrate at high frequencies, from 100 GHz to 2 THz.

From the time-domain electric field, see Fig. 4, provided by the THz-TDS spectroscopic method, we obtain its THz spectrum, see Fig. 5, by applying the FFT on the time signal. Hence, we obtain information of both the amplitude and the phase of the THz waves in the frequency domain.

By analyzing the time-domain electric field (Fig. 4), we observe that a monolayer MoS_2 on sapphire substrate causes a 5.68% decrement at the maximum value of the temporal pulse, as we see in the inset.

Since water has a strong absorption in many of the frequency bands in the THz range, a high relative humidity of the environment would therefore greatly affect the frequency spectra at certain frequencies. The water absorption of the THz wave causes an absorption peak in the frequency spectra of the measured temporal electric field (Fig. 5).

Transmittance represents the intensity portion of the THz wave transmitted through a material and air is used as the transmission reference. Hence, transmittance is defined as the ratio between the frequency-domain wave transmitted through the sample and the reference wave, as

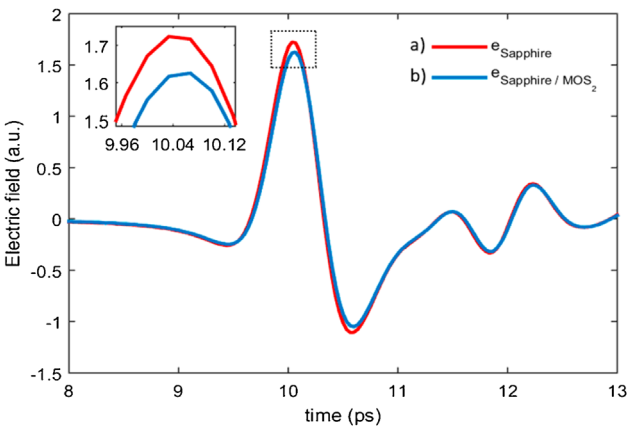

Figure 4 Time-domain electric field pulse of the transmitted THz wave through (a) the bare sapphire substrate and (b) the MoS_2 grown on a sapphire surface, corresponding to sample S_2.

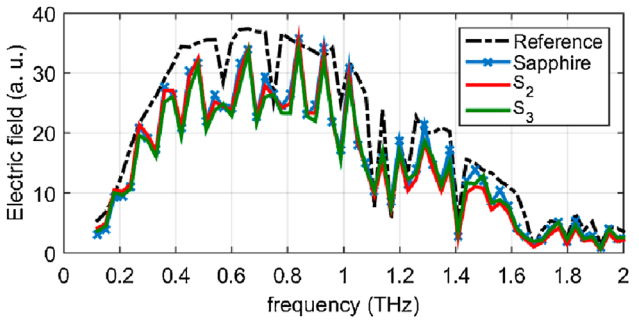

Figure 5 Frequency spectrum of the measured temporal electric field pulse of the transmitted THz wave through the reference (air), the bare substrate (sapphire) and the MoS_2 grown on a sapphire surface, corresponding to samples S_2 and S_3.

follows:

$$T(\omega) = \frac{\mathrm{FFT}[e(t)]}{\mathrm{FFT}[e(t)_{\mathrm{reference}}]}. \quad (1)$$

MoS_2 and graphene transmittances (Fig. 6) are retrieved by using the ratio of the sample (material and substrate) and the bare substrate transmittance:

$$T(\omega)_{\mathrm{material}} = \frac{T(\omega)_{\mathrm{material+substrate}}}{T(\omega)_{\mathrm{substrate}}}. \quad (2)$$

The internal Fabry–Pérot reflections, related to the substrate thickness, cause a set of the oscillations, as seen on Fig. 6.

Graphene (S_1) transmittance in the THz region ranges from 87 to 93% approximately, whereas CVD-S and CVD-H_2S MoS_2 (S_2 and S_3, respectively) show a transmittance close to 95%.

Using the transmittance of the sample and the bare substrate, we are able to determine a large set of optoelectronic properties, such as the complex refractive index (Fig. 7), the sheet conductivity of graphene and MoS_2 (Fig. 8), and their attenuation (Fig. 9), among others [11, 15].

First, we characterize the complex refractive indices, see Fig. 7, of the PET and sapphire substrates, by

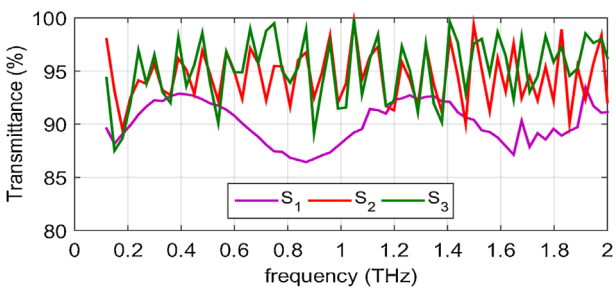

Figure 6 MoS_2 and graphene transmittance. On the left, from top to bottom: (S_2) CVD-S MoS_2 on sapphire, (S_3) CVD-H_2S MoS_2 on sapphire and (S_1) CVD graphene on PET.

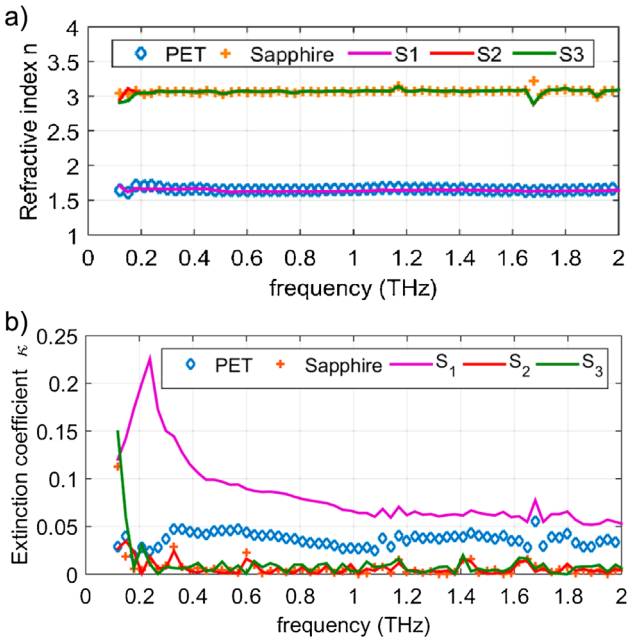

Figure 7 (a) Real part of the refractive indices and (b) imaginary part of the refractive indices of the substrates and the samples composed of the material grown onto the substrate surface. On the left, from top to bottom: sapphire, (S_2) CVD-S MoS_2 on sapphire, (S_3) CVD-H_2S MoS_2 on sapphire, graphene on PET (S_1) and PET.

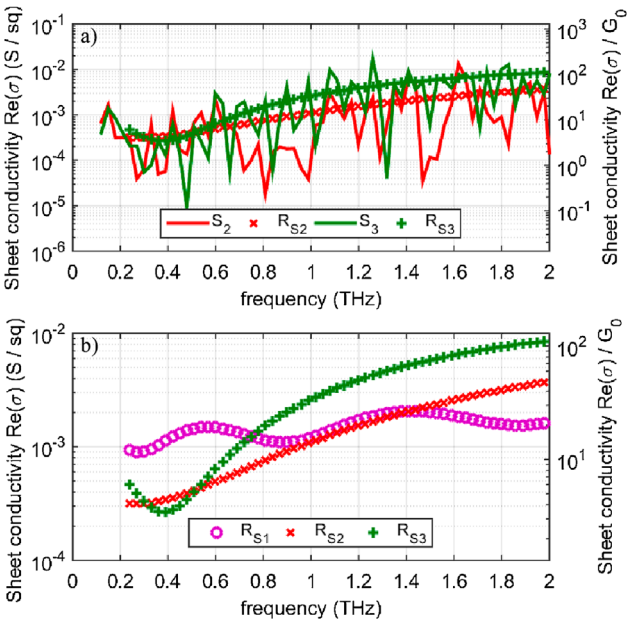

Figure 8 Real part of sheet conductivity of MoS_2 and graphene. (a) Sheet conductivity of: CVD-S MoS_2, S_2, and CVD-H_2S MoS_2, S_3. RS_2 and RS_3 are a graphical representation of the smooth curve that shows the tendency of the sheet conductivity of CVD-S and CVD-H_2S MoS_2, respectively. (b) On the left, from top to bottom: smooth curve of real part of sheet conductivity of (S_1) CVD graphene on PET, (S_3) CVD-H_2S MoS_2 on sapphire and (S_2) CVD-S MoS_2 on sapphire.

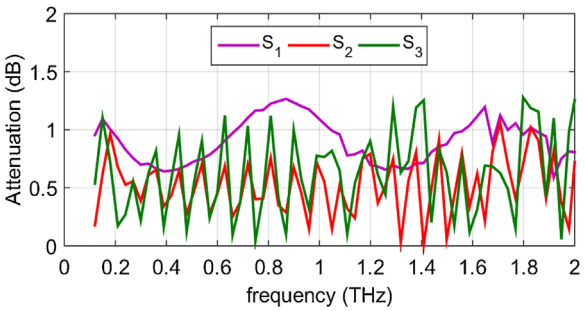

Figure 9 Attenuation of MoS_2 and graphene. On the left, from top to bottom: (S_1) CVD graphene on PET, (S_3) CVD-H_2S MoS_2 on sapphire and (S_2) CVD-S MoS_2 on sapphire.

comparing the substrate signal spectrum with the reference (air) spectrum, whereas we minimize the internal Fabry–Pérot reflection effects produced in thin films [15]. With the complex refractive index, we are able to characterize the substrate and then, we can evaluate the sheet conductivity of MoS_2 and graphene [15] as seen on Table 2.

We found that by growing MoS_2 or transferring graphene onto the bare substrate surface, see Fig. 7a, has no bearing on the values of the sample refractive index.

We deduced the sheet conductivity of MoS_2 and graphene deposited on their respective substrates. To obtain the MoS_2 and graphene conductivity, we have treated them as boundary condition with finite sheet conductivity [15]:

$$T(\omega) = \frac{4\chi \cdot n_{\text{sub}}}{n_{\text{sub}}+1}\exp(-j(n_{\text{sub}}-1)k_0 d_{\text{sub}}) \times \sum_{\text{FP}=0}^{N}\left(\exp(-2jn_{\text{sub}}k_0 d_{\text{sub}})\frac{n_{\text{sub}}-1}{n_{\text{sub}}+1}(2n_{\text{sub}}\chi-1)\right)^{\text{FP}}, \quad (3)$$

where $\chi^{-1} = 1 + n_{\text{sub}} + \sigma_s Z_0$; n_{sub} and d_{sub} are the substrate complex refractive index and thickness, respectively; k_0 is the free-space wave number, Z_0 is the free-space impedance, σ_s is the surface conductivity of the thin film, and FP corresponds to the internal Fabry–Pérot reflections. As the sample thickness is about a hundred μm, we can consider that infinite internal reflections occur in a thin layer, and Eq. (3) can be simplified by

$$T(\omega) = \frac{4\chi \cdot n_{\text{sub}}}{n_{\text{sub}}+1}\exp(-j(n_{\text{sub}}-1)k_0 d_{\text{sub}}) \times \frac{1}{1-\exp(-2jn_{\text{sub}}k_0 d_{\text{sub}})\frac{n_{\text{sub}}-1}{n_{\text{sub}}+1}(2n_{\text{sub}}\chi-1)}. \quad (4)$$

Finally, with all the parameters known, we can extract the MoS_2 and graphene conductivity, see Fig. 8, reported on the right by its normalized conductance quantum units, denoted by the symbol G_0, defined as the quantum unit of electrical conductance:

$$G_0 = \frac{2e^2}{h} \approx 77.48\ \mu\text{S}. \quad (5)$$

As seen in Fig. 8, CVD pristine graphene presents a sheet conductivity around 12–25× the value of quantum conductance, G_0, at frequencies of THz, as expected from previous studies [16, 17]. MoS_2, on the other hand, has a slight difference in values depending on the growth conditions. CVD-S MoS_2, S_2, shows a sheet conductivity around 4.5–42× the value of G_0, whereas CVD-H_2S MoS_2, S_3, presents values 1.3–3 times greater than CVD-S, in the range from 3.4–130× the value of G_0.

By comparing graphene and MoS_2, we observed some different results depending on the frequency range. Specifically, at frequencies below to 750 GHz, graphene sheet conductivity is only marginally higher than both CVD-S and CVD-H_2S MoS_2. From 1 to 1.5 THz, CVD-S MoS_2 sheet conductivity is similar to that of graphene. Finally, at frequencies greater than 1.5 THz, both CVD-S and CVD-H_2S MoS_2 sheet conductivities are slightly higher, up to three times, than that of graphene.

We obtained the attenuation of both MoS_2 and graphene. Attenuation is defined as the intensity loss wave propagation, as follows:

$$A(\omega) = 20\log_{10}(|T(\omega)|). \quad (6)$$

Attenuation of graphene and MoS_2 are illustrated on Fig. 9. We found that CVD pristine graphene, S_1, presents an attenuation from 0.6 to 1.2 dB, whereas MoS_2 shows an attenuation below than 1.8 dB, in detail, CVD-S MoS_2 attenuation, S_2, takes values from 0.1 to 1.7 dB and CVD-H_2S MoS_2, S_3, from 0.1 to 1.8 dB.

3.3 Infrared spectroscopy We studied MoS_2 transmittance in the infrared band, see Fig. 10, in the range from

Table 2 Real part of refractive indices of the substrates, sheet conductivity's smooth values and normalized sheet conductivity of the material σ_s (in mS) and normalized sheet conductivity's smooth values σ_n of the material at 1, 1.5, and 2 THz, normalized to the conductance quantum, G_0.

substrate	sample	growth	material	n	σ_n (1 THz)	σ_s (1 THz)	σ_n (1.5 THz)	σ_s (1.5 THz)	σ_n (2 THz)	σ_s (2 THz)
PET	S_1	CVD	graphene	1.65	15.28	1.18	25.98	2.01	20.89	1.62
sapphire	S_2	CVD-S	MoS_2	3.07	13.93	1.08	29.59	2.29	47.95	3.72
sapphire	S_3	CVD-H_2S	MoS_2	3.07	32.89	2.55	75.14	5.82	109.39	8.48

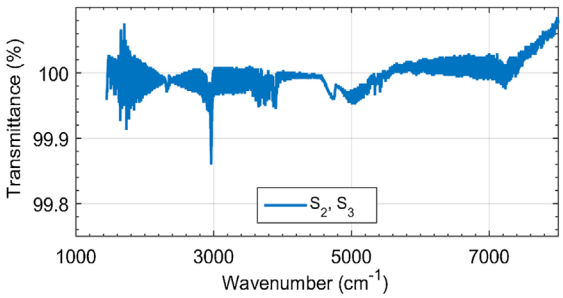

Figure 10 IR transmittance of MoS_2.

400 to 8000 cm^{-1}. Graphene IR spectroscopy is reported in Ref. [11]. Spectra have been collected with the Frontier FT-IR/FIR Spectrometer from Perkin Elmer at CCiTUB.

It is important to emphasize that, as the MoS_2 transmittance is extracted by comparison (Eq. (2)) using substrate transmittance, we can only determine the material transmittance as long as the transmittance of both the sample and the bare substrate are not null. Therefore, because the sapphire transmittance is null at wave numbers below 1700 cm^{-1}, we can only study the transmittance of MoS_2 in the range from 1700 to 8000 cm^{-1}, where MoS_2 present values of transmittance close to 99.8%, see Fig. 10.

4 Discussion and conclusions We have characterized the electronic properties of CVD MoS_2 and graphene over the THz and IR ranges.

We studied the electronic properties of CVD monolayers of MoS_2 depending on the growth conditions, by controlling the growth direction of MoS_2 domains using H_2S as a gas-phase precursor (CVD-H_2S), in addition to conventional sulfur (CVD-S).

We found that CVD-S MoS_2 presents a sheet conductivity of 4.5–42× the value of quantum conductance, G_0, whereas CVD-H_2S MoS_2 presents values in the range from 3.4–130× the value of G_0, while graphene shows a sheet conductivity around 12–25× the value of G_0. Therefore, we found that the CVD monolayer MoS_2 sheet conductivity, at frequencies in the range 1–2 THz, is up to three times greater for MoS_2 obtained using H_2S as a sulfur gas precursor than the usual CVD MoS_2 obtained with sulfur. This is probably because the former is more ordered.

The attenuation on variously obtained MoS_2 in the THz range are presented, and for comparison, also the graphene attenuation. We observed that monolayer MoS_2 shows an attenuation below 1.8 dB. In comparison, graphene presents an attenuation from 0.6 to 1.2 dB, similar to MoS_2.

The study of a material transmittance is a key factor to characterize a material over a wide frequency range. We found that at THz frequencies, from 100 GHz to 2 THz, the CVD-S and CVD-H_2S MoS_2 transmittance is close to 95%, similar to that of graphene. On the other hand, at IR wave numbers, CVD-S an CVD-H_2S MoS_2 transmittance is close to 99.8%. Therefore, the use of MoS_2 is very promising in the development of optoelectronic devices, with similar properties to those of graphene. Moreover, the existing bandgap in MoS_2 will provide the possibility to achieve transistors for flexible or transparent electronics.

Acknowledgements The authors thank the CCiTUB services for Raman, IR and the AntennaLAB group from Department of Signal Theory and Communications of UPC. The work of D. Dumcenco and A. Kis was financially supported by funding from the Swiss SNF Sinergia grant no. 147607. The work of D. Dumcenco was carried out in the framework of the Marie Curie ITN network "MoWSeS" (grant no. 317451). We acknowledge partial funding by the EC under the Graphene Flagship (grant agreement no. 604391).

References

[1] Y. Lee, X. Zhang, W. Zhang, M. Chang, C. Lin, K. Chang, Y. Yu, J. T. Wang, C. Chang, and L. Y. L. T. Li, Adv. Mater. **24**(17), 2320–2325 (2012).
[2] W. Zhu, T. Low, Y. Lee, H. Wang, D. B. Farmer, J. Kong, F. Xia, and P. Avouris, Nature Commun. **5**, 3087 (2014).
[3] B. Radisavljevic, A. Radenovic, J. Brivio, V. Giacometti, and A. Kis, Nature Nanotechnol. **6**(3), 147–150 (2011).
[4] O. Lopez-Sanchez, D. Lembke, M. Kayci, A. Radenovic, and A. Kis, Nature Nanotechnol. **8**(7), 497–501 (2013).
[5] K. F. Mak, C. Lee, J. Hone, and J. Y. H. T. F. Shan, Phys. Rev. Lett. **105**(13), 136805 (2010).
[6] S. Ahmad and S. Mukherjee, Graphene **3**(4), 52–59 (2014).
[7] M. Tonouchi, Nature Photon. **1**(2), 97–105 (2007).
[8] X. Zhang and J. Xu, Introduction to THz Wave Photonics (Springer, New York, 2010).
[9] M. F. Khan, M. Z. Iqbal, M. W. Iqbal, V. M. Iermolenko, H. M. Waseem Khalil, J. Nam, K. S. Kim, H. Noh, and J. Eom, RSC Adv. **5**(62), 50040–50046 (2015).
[10] D. Dumcenco, D. Ovchinnikov, O. Lopez Sanchez, P. Gillet, D. T. L. Alexander, S. Lazar, A. Radenovic, and A. Kis, 2D Mater. **2**(4), 044005 (2015).
[11] D. Gabriel, B. Sempere, C. Colominas, and N. Ferrer-Anglada, Phys. Status Solidi B **252**(11), 2423–2428 (2015).
[12] H. Li, Q. Zhang, C. C. R. Yap, B. K. Tay, T. H. T. Edwin, A. Olivier, and D. Baillargeat, Adv. Funct. Mater. **22**(7), 1385–1390 (2012).
[13] B. Chakraborty, A. Bera, D. V. S. Muthu, S. Bhowmick, U. V. Waghmare, and A. K. Sood, Phys. Rev. B **85**(16), 161403 (2012).
[14] D. Dumcenco, D. Ovchinnikov, K. Marinov, P. Lazić, M. Gibertini, N. Marzari, O. L. Sanchez, Y. Kung, D. Krasnozhon, M. Chen, S. Bertolazzi, P. Gillet, A. Fontcuberta I Morral, A. Radenovic, and A. Kis, ACS Nano **9**(4), 4611–4620 (2015).
[15] M. Liang, M. Tuo, and H. Xin, Terahertz characterization of carbon nanotube and graphene on-substrate thin films, in: 7th European Conference on Antennas and Propagation (EuCAP), Gotenburg, 2013.
[16] W. Liu, R. V. Aguilar, Y. Hao, R. S. Ruoff, and N. P. Armitage, J. Appl. Phys. **110**(8), 083510 (2011).
[17] N. Rouhi, D. Jain, S. Capdevila, L. Jofre, E. Brown, and P. J. Burke, Broadband conductivity of graphene from DC to THz, in: 11th IEEE International Conference on Nanotechnology, Portland, Oregon, USA, 2011.